PCCP

Accepted Manuscript

ROYAL SOCIETY OF CHEMISTRY

www.rsc.org/pccp

Physical Chemistry Chemical Physics

ARTICLE

Squaraine based Solution Processed Inverted Bulk Heterojunction Solar Cells Processed in Air

Received 00th January 20xx,
Accepted 00th January 20xx

DOI: 10.1039/x0xx00000x

www.rsc.org/

P. C. Reshmi Varma[a] and Manoj A. G. Namboothiry[a]*

Inverted bulk heterojunction solar cells based on low temperature solution processed squaraine (SQ) and [6,6]-phenyl C_{71} butyric acid methyl-ester ($PC_{71}BM$) with varying blend ratios were made in air. Optimized bulk hetero junction device of SQ and $PC_{71}BM$ (Blend ratio of 1:6) showed a power conversion efficiency (PCE) of 2.45% with an incident photon to current conversion efficiency of 65% at 680 nm and a spectral window, extending to NIR region. The devices also showed an enhanced PCE value of 4.12% upon continuous illumination of AM1.5G light source of intensity 1 sun. The intensity dependent photocurrent studies showed a monomolecular recombination mechanism in the photovoltaic device performance. The device stored in air showed reasonable stability for a period of one month.

Introduction

Squaraines (SQN) are a class of small molecular organic dye which were reported in 1965[1] and are widely used in different applications such as sensing,[2] imaging,[3] nonlinear optics,[4,5] photovoltaic[6,7] etc. Small molecule based high performance photovoltaic research has gained significant momentum during the last few years due to its advantages, such as intrinsically monodispersive, easy to synthesize with a good batch to batch reproduction, ease of purification[8,9] and easily controlled band gap compared to polymers. It is also to be noted that the effect of parameters such as regioregularity, polydispersity and stability on polymer based photovoltaic devices have not been fully understood. SQN with all the properties of a small molecule is a promising candidate to be used as an active donor material in small molecule based organic photovoltaics (OPV). SQN also shows a broad spectral response extending to the near infrared (NIR) wavelength (λ) region (450 nm < λ < 800 nm),[10] large absorption coefficient (α ~ 3×10^5 cm^{-1})[11] and stability, which are advantageous to OPV performances. Initial SQN based OPV devices used a bilayer structure with thermally evaporated SQN as a donor and Phenyl-C_{61}-butyric acid methyl ester ($PC_{61}BM$) as an acceptor layer.[12] Since the exciton diffusion length was very low (L_D < 5 nm), an interpenetrating bulk heterojunction (BHJ) approach was used by co-thermal deposition of SQN and [6,6]-phenyl C_{71} butyric acid methyl-ester ($PC_{71}BM$) to improve the exciton dissociation.[13] In order to improve the ease of OPV fabrication and keeping in mind the role to role processing of OPV, solution processed SQN were developed and BHJ devices were made using spin coating of different ratios of SQN:C_{60} or C_{70} blend solutions.[14-16] Various interfacial layers were used to enhance the power conversion efficiencies of such BHJ devices. Molybdenum trioxide (MoO_3) and Poly(3,4-ethylenedioxythiophene)-poly (styrene sulfonate) (PEDOT:PSS) are some of the hole transporting materials commonly used as buffer layers at the Indium tin oxide (ITO)/Polymer or ITO/small molecule interface. But due to their highly hygroscopic nature, these materials can induce damage to ITO/PEDOT:PSS or ITO/MoO_3 interfaces and can introduce high series resistance to the OPV. As an alternative route, inverted solar cell structures were introduced to counter such deteriorating factors. To the best of our knowledge there have not been any reports to date of any application of inverted geometry in solution processed BHJ of SQN based devices.

Even though SQN is an air stable material, most of the devices reported in literature were made in controlled atmosphere. For the development of a cost effective fabrication technology, it is highly desirable to develop processes under normal atmospheric conditions without affecting device performance. In this article, we study the inverted solution processed BHJ OPV made from 2,4-Bis[4-(N,N-diisobutylamino)-2,6-dihydroxyphenyl] squaraine (SQ) and $PC_{71}BM$ (Fig 1a, Fig 1b) using normal atmospheric processing. The inverted solar cells were fabricated using the configuration ITO/PFN/SQ:PCBM/MoO_3/Al. Poly [(9,9-bis(3´-(N,N-dimethylamino) propyl)-2,7-fluorene)-alt-2,7-(9,9–dioctylfluorene)] (PFN) (Fig.1c) was used as an interfacial layer between ITO and SQ:$PC_{71}BM$ blend as it modifies the work function of ITO so that it can be used as cathode in inverted solar cell.[17,18] The low temperature solution processing property of PFN is advantageous compared to high temperature processed metal

[a] School of Physics, Indian Institute of Science Education and Research Thiruvananthapuram, CET Campus, Engineering College P O, Thiruvananthapuram, Kerala, India. PIN 695016
*Email: manoj@iisertvm.ac.in

† Footnotes relating to the title and/or authors should appear here.
Electronic Supplementary Information (ESI) available: [Comparison of UV VIS absorbance data of pristine SQ and SQ:PCBM blend of same thickness, SCLC fitting of dark IV characteristics of hole only devices, Dark I-V characteristics of devices and rectification ratio .of the devices]. See DOI: 10.1039/x0xx00000x

oxide as interfacial layer for large area applications and flexible substrates. The device structure and the energy level diagram are shown in Fig.1d, Fig.1e.

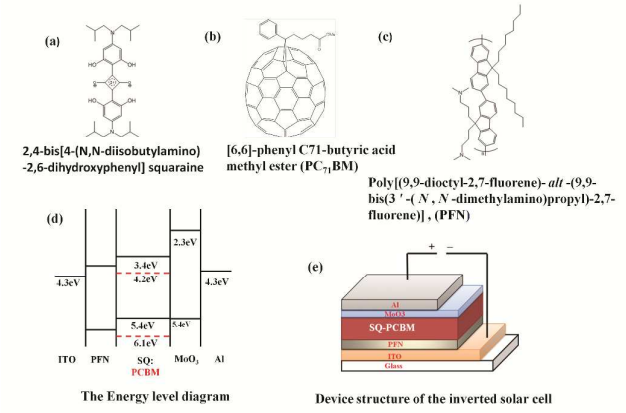

Fig.1 Molecular structure of (a) Squaraine, (b) $PC_{71}BM$, (c) PFN. Schematic of (d) the Energy level diagram (e) the device structure of the inverted solar cell.

Experimental Section

Materials and methods

All the chemicals and the substrates used for the fabrication were commercially purchased. The devices were fabricated on cleaned indium tin oxide (ITO) coated glass plates (10 Ω/cm^2, Delta Technologies Inc, USA). Poly [(9,9-bis(3′-(N, N -dimethylamino) propyl)-2,7-fluorene)- alt -2,7-(9,9–dioctylfluorene)] (PFN, Purity > 99%, 1 Materials Canada) was used to modify the work function of ITO to be used as cathode in the inverted structure. Active layers were made using different blend ratios of 2,4 bis[4-(N,N-diisobutylamino)-2,6-dihydroxyphenyl] squaraine (SQ, Purity > 99%, Sigma Aldrich) and [6,6]-phenyl C_{71} butyric acid methyl-ester ($PC_{71}BM$, Purity > 99%,American Dye Sources, Canada) in ortho-dichlorobenzene (ODCB, Sigma Aldrich, HPLC grade). Thermally evaporated molybdenum trioxide (MoO_3, Purity > 99%, Sigma Aldrich) were used as a hole transporting, electron blocking interfacial layer. Aluminum was used as the back contact which was purchased from Sigma Aldrich.

Device Fabrication and Characterization.

Devices were fabricated on ITO coated glass substrate. ITO coated glass plates were cleaned with soap solution and ultrasonicated using deionized water, acetone and isopropyl alcohol for 30 minutes respectively. Cleaned substrates were kept in vacuum oven over night for drying. Before spin coating the layers, ITO samples were exposed to UV Ozone for about 30 minutes. On top of ITO substrates, PFN was spin coated, which was dissolved in methanol mixed with acetic acid with a concentration of 0.2 mg/ml was spin coated at an rpm of 2000 to obtain a thin film of ~5 nm and is used as an electron transporting, hole blocking layer. Active layers were made using different blend ratios of SQ: PCBM keeping a constant solution concentration (42mg/ml) to obtain a uniform thickness of active layer over different devices. Active layer solution was then spin coated (1500 rpm) over thin PFN layer to form a layer of thickness 100 nm. Thin layer of (7nm) MoO_3 evaporated at a pressure of ~10^{-6} torr were used as a hole transporting, electron blocking interfacial layer. Aluminum (Al) of thickness ~100 nm was thermally evaporated at a base pressure of 10^{-6} torr and is used as the top electrode. A device structure of ITO/PFN/SQ:$PC_{71}BM$/MoO_3/Al were made for the solar cell studies. The thickness of spin cast films was measured using a Dektak stylus profilometer and that of thermally evaporated materials using an Inficon thickness monitor. The active area of the device was 9 mm^2. The devices were unencapsulated and all the measurements were performed in ambient conditions with samples mounted on a temperature controlled chuck. The sample temperature is maintained at 25^0 C and is monitored using a thermocouple.

The current-voltage characteristics of the devices were done with Keithley 6430 source meter in dark and under the illumination of 1000 W/m^2 AM1.5G spectrum using Oriel 3A solar simulator tested with a NREL calibrated silicon solar cell. The external quantum efficiency (EQE) measurements were done using lockin technique with a 250 W xenon lamp coupled with a Newport monochromator and chopped at 40 Hz with a light chopper blade as light source. A lockin amplifier (SRS 830, Stanford Research Systems Inc USA) was used to measure currents and a NIST calibrated silicone photodiode was used to find the power spectral response of the incident light. The measurements were done using shadow masks to avoid edge effects and proper mismatch factor was taken to square off the spectral mismatch while calculating PCE and EQE.[19,20]. The intensity dependent measurements were done using AM1.5G, 1 Sun light source, in combination with neutral density filters of different optical density.

Result and discussion

Different SQ:$PC_{71}BM$ ratios were tested to derive the best performance by considering high absorption coefficient, broad spectral window extending up to λ ~ 800 nm and low exciton diffusion length < 6 nm of SQ and large diffusion length and poor absorption coefficient of $PC_{71}BM$.

The best results were obtained for an active layer of ~100 nm thickness made from 1:6 blend ratios by weight of SQ: $PC_{71}BM$ with an external quantum efficiency (EQE), varying from 45% to 65% in the spectral window extending to λ ~ 800 nm and power conversion efficiency (PCE) of 2.45%. We fabricated more than 20 devices in each ratio and more than 50 of best performing devices with SQ:$PC_{71}BM$ blend ratio of 1:6 by weight. The performance of organic photovoltaic cells depends on many parameters such as efficient light absorption, exciton creation, exciton dissociation, free carrier transport, and charge transfer to the electrodes. In order to understand the above mentioned factors, various electrical and optical measurements were carried out.

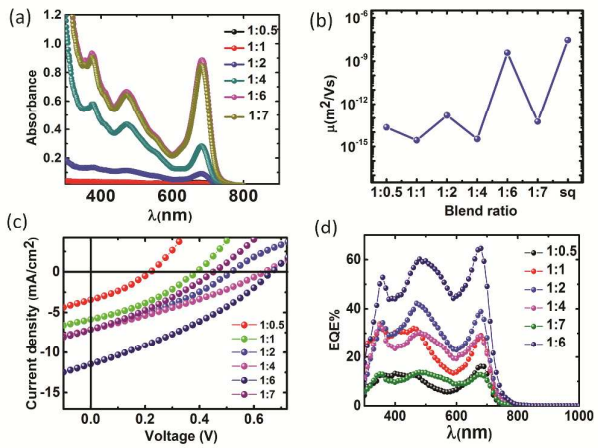

Fig. 2 (a) UV-Vis absorption of different ratios of SQ:$PC_{71}BM$ blend (b) Hole mobility of squaraine in pristine film and in blend with $PC_{71}BM$ in different ratios (c) Current density vs Voltage (J-V) characteristics of the SQ:$PC_{71}BM$ devices for different blend ratios, , (d) EQE of SQ:$PC_{71}BM$ devices fabricated in different blend ratios

The UV VIS absorption spectra of SQ:$PC_{71}BM$ of different blend ratio is as shown in Fig 2 a. It is to be noted that we have measured the absorption spectra of thin films of same thickness (100 nm) as we used in our devices for different blend ratio. The absorption strength of SQ at λ ~ 683 nm steadily increases as SQ:$PC_{71}BM$ blend ratio is varied from 1:0.5 to 1:6. This is in spite of the fact that the weight content of SQ in 1:6 blend ratio is much less than that in blend ratio of 1:0.5. This may be due to the well-known fact that SQ dimers or aggregates show less absorption coefficient compared to monomers.[21] Or in other words, in SQ:$PC_{71}BM$ blend ratio of 1:6, SQ is well dispersed in $PC_{71}BM$ matrix with monomer like features and in other blends it is in dimeric or in aggregate form. A comparison of UV VIS absorbance of pristine SQ thin films of 100 nm thickness with that of SQ:PCBM blends (1:0.5 blend ratio) is given as Fig S1. This clearly shows the aggregation of SQ with a broadened absorption spectrum and reduced absorbance of SQ only thin films compared to SQ:PCBM blends.

Along with other parameters, a balanced electron and hole mobility of $PC_{71}BM$ and SQ respectively are necessary to extract free carriers from the BHJ devices. In order to find the best blend ratio for achieving balanced hole and electron transport, SQ:$PC_{71}BM$ of different blend ratios were studied. SQ shows hole mobility of $2.83 \times 10^{-4} cm^2/Vs$ in pristine form and it further reduces in conjunction with $PC_{71}BM$. Hole mobility of SQ in the blend film is controlled by the hopping of hole through the SQ domains in the blend.[22] Previous reports of zero field mobility of SQ suggest that the performances of the SQ:$PC_{71}BM$ blend was limited by poor hole mobility through the discontinuous SQ networks compared to the electron mobility through $PC_{71}BM$ networks.[14] We also observe a similar result with SQ:$PC_{71}BM$, 1:6 blend ratio, showing a hole mobility nearer to that of pristine SQ compared to other SQ:$PC_{71}BM$ blend ratios. The improved hole mobility of SQ in SQ:$PC_{71}BM$ of blend ratio 1:6 can be attributed to well dispersed SQ in $PC_{71}BM$ matrix with SQ within the optimized hopping distance[22]. This argument is speculated based on the SQ contribution to UV VIS absorption of different SQ:$PC_{71}BM$ blend ratios and mobility studies. Fig. 2b shows the variation of hole mobility of SQ in different blend ratios of $PC_{71}BM$. We find that SQ:$PC_{71}BM$ of 1:6 blend ratio has the hole mobility much near to the electron mobility of $PC_{71}BM$[23,24] and expected to show better OPV performances. Measurement of hole mobility of SQ is done by using a hole only device of ITO/PEDOT-PSS/SQ/Au and ITO/PEDOT-PSS/SQ:$PC_{71}BM$/Au. Mobilities were calculated by fitting the dark IV characteristic with a space charge limited current (SCLC) model. Equation 1 (Fig S2).

$$J = \frac{9}{8}\varepsilon_0 \varepsilon \mu_h \frac{V^2}{L^3} \quad (1)$$

Where ε_0 is the permittivity of free space, ε is dielectric constant of the organic material, we assumed ε=3[25] , V is the applied voltage, L is the thickness of the layer and μ_h is the mobility.

Devices with different SQ:$PC_{71}BM$ blend ratio by weight was fabricated and tested for its photovoltaic properties. The dark I-V and rectification ratio is as shown in Figure S3 and Table S1 respectively. The I-V characteristics of the inverted BHJs for different ratios of SQ:$PC_{71}BM$ in presence of light are shown in Fig.2c. The open circuit voltage (V_{OC}), short circuit current density (J_{SC}) and power conversion efficiency (PCE) increases as the SQ:$PC_{71}BM$ ratio varies from 1:0.5 to 1:6 and further it remains constant or deteriorates. The origin of such improvement leading to an increase in V_{OC}, J_{SC} and PCE to 0.68 V, 11.47 mA/cm^2, and 2.45%, respectively, for an optimized SQ:$PC_{71}BM$ blend ratio of 1:6 depend on effective transport and transfer of free carriers created upon exciton dissociation in the BHJ OPV.

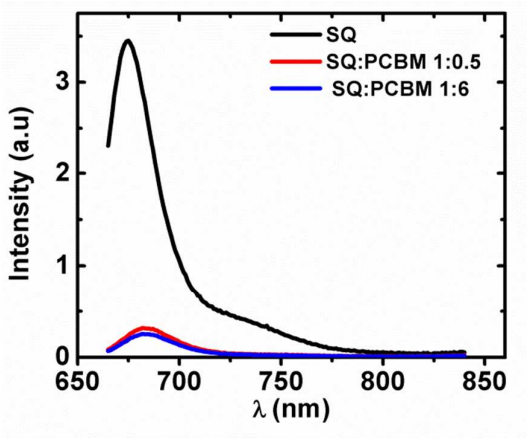

Fig. 3 PL spectra of thin films of pristine SQ , SQ:PCBM blends of blend ratio 1:0.5 and 1:6 excited at 600 nm.

Photoluminescence (PL) quenching experiments of SQ in presence of $PC_{71}BM$ shows a good quenching of the PL peak of SQ at λ ~ 688 nm (Fig.3) even with a small amount of PCBM. The quenching does not vary much with higher PCBM content. This shows an efficient exciton quenching at SQ:$PC_{71}BM$ interface. EQE of the devices with different blend ratios provide information about the effective extraction of free carriers created by the exciton dissociation at different λ in the spectral window of SQ:$PC_{71}BM$ blend.

The EQE of the inverted BHJ OPVs with different blend ratio of SQ and $PC_{71}BM$ is as shown in the Fig. 2d. The EQE shows added contribution from both SQ and $PC_{71}BM$. By comparing the EQE vs. λ spectra with absorption spectra (Fig. 2a) of individual SQ and $PC_{71}BM$, it can be inferred that the photocurrent in the λ range 300 nm to 600 nm is mostly due to $PC_{71}BM$ with peaks at λ =360 nm, λ = 484 nm and photocurrent up to λ ~ 800 nm is mostly due to SQ with a peak at λ ~ 680 nm. The EQE of the device increases steadily as the SQ:$PC_{71}BM$ blend ratio is varied from 1:0.5 to 1:6, and for the higher PCBM weight ratio, it reduces. The optimized performance of the SQ:$PC_{71}BM$ blend ratio of 1:6 can be due to a balanced electron and hole transport. Deviation from this blend ratio results in a poor charge extraction and reduced EQE**.** This is inferred from the following observations. [a) if the exciton dissociation was the dominant EQE mechanism, the EQE at λ ~ 680 nm should have increased or remained the same as the absorption of SQ increases in the blend as the SQ:$PC_{71}BM$ blend ratio is increased from 1:0.5 to 1:7. But here we observe a decrease in EQE at λ ~ 680 nm as the SQ:$PC_{71}BM$ blend ratio Is increased from 1:6 to 1:7. This can be attributed to an imbalanced mobility of electron and hole in the blend as the hole mobility of SQ is reduced significantly as the SQ:$PC_{71}BM$ blend ratio is varied from 1:6 to 1:7 (which is measured using SCLC method as shown in Fig 2 b), b) EQE spectra show peaks at λ ~ 360 nm, λ ~ 490 nm and λ ~ 680 nm similar to the absorption peaks of the blend. Most of the light get absorbed near the PFN /blend interface in the wavelength range 300 nm < λ < 400 nm and at MoO_3/blend interface in the wavelength range 600 nm < λ < 800 nm. We expect a bigger ratio of EQE at λ ~ 360 nm with respect to λ ~ 680 nm, in similarity with absorption profile. But, here we observe a reduced ratio. This can be due to recombination of holes created at the PFN/Blend interface before reaching the MoO_3/blend interface due to mobility mismatch between holes and electrons in the blend. In the case of EQE at λ ~ 680 nm and λ ~ 490 nm, holes are created much near the MoO_3/blend interface and can be easily extracted to MoO_3, without much recombination. On the other hand, the electrons created at MoO_3/blend interface do not face much recombination as it can be easily transported through $PC_{71}BM$ to PFN/blend. This explains 1) the < 1 ratio of EQE at λ ~ 360 nm with respect to that at λ ~ 680 nm compared to its > 1 ratio of absorption at respective wavelengths, 2) comparable EQE and absorption ratios for λ ~ 490 nm with respect to λ ~ 680 nm.] . Our results are in agreement with previous reports where it is mentioned that the EQE mostly depend on the balanced electron and hole mobility in the blend rather than the exciton dissociation.[14] For the highest efficiency device (1:6) the average efficiency is about 55% through the UV-Vis and NIR region. The peak efficiency was 65% at λ ~ 680 nm. The J_{SC} calculated for the highest efficiency device from EQE spectra by multiplying the EQE spectra by the standard AM1.5G and integrating it over the wavelength region was in good agreement with the J_{SC} from current voltage (I-V) experiments in presence of AM 1.5G light of intensity 1 Sun. The calculated J_{SC} was 11.67 mA/cm^2, whereas the experimentally (I-V) obtained value for the respective devices was 11.47 mA/cm^2.

The V_{OC} of devices with different ratios of SQ:$PC_{71}BM$ are given in Table 1. The V_{OC} increases with increasing $PC_{71}BM$ and an optimum V_{OC} of 0.68 V is observed for devices with SQ:$PC_{71}BM$ blend ratio of 1:6. Further increase in $PC_{71}BM$ content decreases the V_{OC}. The extraction of free carriers from the devices increases as the SQ:$PC_{71}BM$ blend ratio is increased from 1:0.5 to 1:6. This can be attributed to reduced recombination due to mismatch between the hole and electron mobility as observed in mobility measurements of SQ:$PC_{71}BM$ of different blend ratios. Hence the improvement in V_{OC} can be a result of limited recombination in the BHJ OPV and a maximum value of 0.68 V is observed for optimized SQ:$PC_{71}BM$ devices of blend ratio 1:6. Further increase in $PC_{71}BM$ content modifies the mobility match between the hole and electron and results in a recombination limited extraction and reduced V_{OC}. The devices also show a similar trend for J_{sc} with an optimized performance of 11.47 mA/cm^2 for SQ:$PC_{71}BM$ devices with a blend ratio of 1:6.

Here, in the best performing device, the photocurrent I_{ph} shows KI^{α} dependence on incident light intensity I (where α is the exponential factor and K a proportionality constant), with α value ~1 (Fig 4 a). This shows the properties of monomolecular or geminate recombination mechanism.[26,27] in the SQ:$PC_{71}BM$ devices. As intensity increases V_{OC} increases and saturates for higher intensities (Fig.4b). The general expression for V_{OC}[28] is given in Equation 2.

$$qV_{OC} = \Delta E_{DA} - \frac{\sigma^2}{k_B T} - k_B T \ln\left(\frac{N_A N_D}{np}\right) \qquad (2)$$

The first term is the effective band gap, ΔE_{DA}, the second term represents disorder induced V_{OC} loss, and the third term represents carrier recombination induced V_{OC} loss. At low intensities n and p vary linearly with intensity as a result V_{OC} varies logarithmically with intensity. At higher intensity shunt resistance (R_{sh}) of the device is reduced[29] and hence the term V/R_{sh} in the practical diode equation for solar cell cannot be neglected (shown in Equation 3.), where T is the temperature,

Table 1. Summary of the Current-Voltage characteristics for different ratios of SQ:$PC_{71}BM$ inverted solar cells under 1 sun illumination

SQ:$PC_{71}BM$ Ratio	V_{OC} (V)	J_{SC} (mA/cm^2)	FF (%)	PCE (%)
1:0.5	0.23	0.34	28.69	0.25
1:1	0.38	5.86	32.12	0.78
1:2	0.53	7.11	28.47	1.18
1:4	0.65	7.10	26.54	1.36
1:6	0.68	11.47	31.62	2.45
1:7	0.53	7.43	28.13	0.99

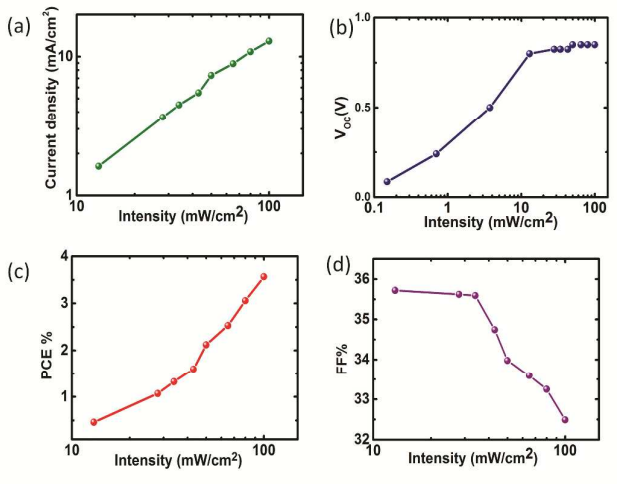

Fig.4 Dependence of (a) J_{SC} (b) V_{OC} (c) PCE% and (d) FF% on Illumination intensity of inverted SQ: $PC_{71}BM$ photovoltaic cells blended at 1:6 ratios

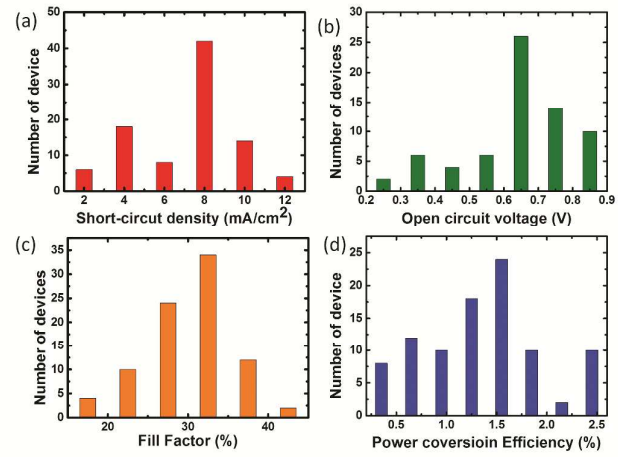

Fig. 5 Histogram of the photovoltaic performance parameters such as (a) J_{SC}, (b) V_{OC}, (c) FF% and (d) PCE% of the SQ:$PC_{71}BM$ (1:6) inverted solar cell

k_B is the Boltzmann constant, m is the diode ideality factor, J_0 is the reverse saturation current density J_{ph} is the photocurrent V is the output voltage, and R_S is series resistance)

.

$$J = \frac{R_{sh}}{R_{sh}+R_s}\left\{J_0\left[\exp\left(\frac{q(V-JR_s)}{mk_BT}\right)-1\right]+\frac{V}{R_{sh}}\right\}-J_{ph} \quad (3)$$

This again causes the reduction in V_{OC}. So at higher intensities, increase of n and p counteracts the reduction in parallel resistance R_{sh} and when these two effects balance, V_{OC} saturates. The FF of the best devices was 31.62% and this low value was attributed to large internal series resistance, which can be due to poor extraction of free carriers. A histogram of the best performing device characteristics is given in Fig. 5.

The optimized inverted BHJ OPV shows an enhanced power conversion efficiency of 4.12% upon exposure of the device to AM1.5G light of intensity 1 sun for 10 minutes, prior to I-V measurements. The PCE vs. exposure time for the device with blend ratio 1:6 is shown in Fig.6a. As the illumination time varies from one to ten minutes PCE increases from 2.45% to 4.12% and further exposure results in a saturation of PCE at 4%. Devices with other blend ratios exhibit similar behaviour. The EQE spectrum of the device before and after illumination shows an increase in EQE over the entire wavelength region without any distortion of spectral shape (Fig. 6b). This increase in PCE and EQE upon exposure of light before the measurement can be explained by the enhanced charge carrier transport through the bulk and transfer to the electrode. The reason for the enhanced performance of the device on continuous exposure of light is arising from the ITO/PFN interface. The devices were fabricated under ambient conditions; the adsorbed oxygen on the ITO caused the formation of the mid gap charge transfer states in the PFN layer near to the ITO/PFN interface.[30] These states increase the work function of ITO by reducing the electric dipole moment within the PFN layer. Up on continuous light exposure, the photon excited electron fills the mid trap states and restores the reduced dipole moment of PFN. This helps to reduce the work function of ITO as well as the charge extraction barrier, hence showing a better performance. This can be attributed to reduced recombination and enhanced free carrier transport as an improved V_{OC} and J_{SC} was observed while doing I-V after light exposure of the devices. Fig.7 gives the variation observed in solar cell parameters with time

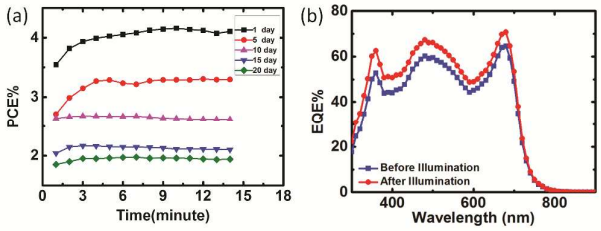

Fig. 6 (a). Illuminated AM1.5G, 1 Sun light exposure time effect on power conversion efficiency of SQ:$PC_{71}BM$ photovoltaic device blended at 1:6 ratio and the stability of the cell tested on different days. b).EQE of the SQ:$PC_{71}BM$ (1:6) device before and after continuous illumination of the device under 1 sun illumination.

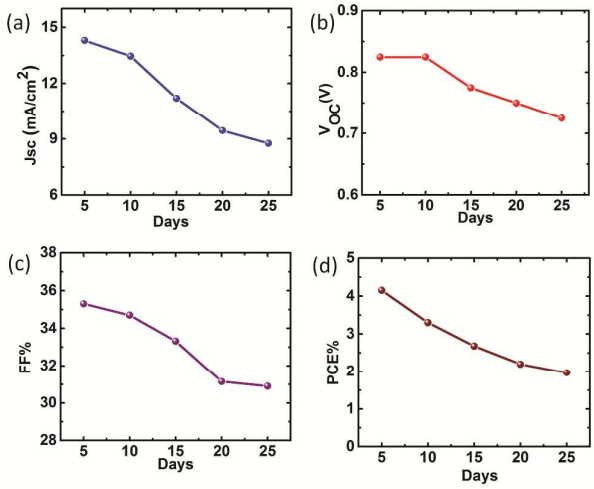

Fig.7 Variation of solar cell parameters (a) J_{SC}, (b) V_{OC}, (c) FF%, (d) PCE% with time

Further work is in progress to understand the origin of such an enhancement. Prolonged measurements of PCE at certain intervals of time after illumination show a small decrease in PCE value. The stability of the devices in air was tested for a period of 1 month. The devices were unencapsulated and characterized under ambient conditions. The devices showed good stability under these conditions, with a decrease in efficiency to 2%.

Conclusions

In conclusion, solution processed inverted SQ:$PC_{71}BM$ devices were fabricated and the ratio was optimized as 1:6 with a power conversion efficiency of 2.45%. The devices also showed an enhanced PCE value of 4.12% upon continuous illumination with AM1.5G light source. The device performance parameters such as V_{OC}, J_{SC}, and EQE were studied in detail and correlated with the spectroscopy studies of SQ in the presence of $PC_{71}BM$. The device showed spectral response with an EQE varying from 45% to 65% over a broad solar spectral window extending to the NIR region. Intensity dependent measurement of devices showed monomolecular recombination as one of the limiting factors of the performance of the device. The air processed device showed reasonable stability for a period of one month

Acknowledgements

We acknowledges funding from Department of Science and Technology (DST/TM/SERI/2k11/73(G)), Solar Energy Research Initiative project, Ministry of Human Resource Development both under Govt. of India.

Notes and references

‡ Footnotes relating to the main text should appear here. These might include comments relevant to but not central to the matter under discussion, limited experimental and spectral data, and crystallographic data.

1 A. Treibs, K. Jacob, *Angew. Chem. Int. Ed*., 1965, 4, 694.
2 A. Ajayaghosh, *Acc. Chem. Res.*, 2005, **38**, 449.
3 A.C. Tam, *Appl. Phys. Lett*., 1980 , **37**, 978.
4 C.W. Dirk, W.C. Herndon, F. Cervantes-Lee, H. Selnau, S. Martinez, P. Kalamegham, A. Tan, G. Campos, M. Velez, *J. Am. Chem. Soc.,* 1995, **117**, 2214.
5 G.J. Ashwell, G. Jefferies, D.G. Hamilton, D.E. Lynch, M.P.S. Roberts, G.S. Bahra, C.R. Brown, *Nature*, 1995, **375** , 385.
6 V.Y. Merritt, H.J. Hovel, *Appl. Phys. Lett*., 1976, **29**, 414.
7 D.L. Morel, A.K. Ghosh, T. Feng, E.L. Stogryn, P.E. Purwin, R.F. Shaw, C., *Appl. Phys. Lett*. , 1978, **32**, 495.
8 B. Walker, C. Kim, T.-Q. Nguyen, *Chem. Mater.,* 2010, **23**, 470.
9 J. Roncali, *Acc. Chem. Res*., 2009, **42**, 1719.
10 S. Sreejith, P. Carol, P. Chithra, A. Ajayaghosh, *J. Mater. Chem*., 2008, **18** , 264.
11 G. Chen, D. Yokoyama, H. Sasabe, Z. Hong, Y. Yang, J. Kido, *Appl. Phys. Lett.,* 2012, **101** , 083904
12 S. Wang, E.I. Mayo, M.D. Perez, L. Griffe, G. Wei, P.I. Djurovich, S.R. Forrest, M.E. Thompson, *Appl. Phys. Lett*., 2009, **94**, 233304.
13 G. Chen, H. Sasabe, Z. Wang, X.-F. Wang, Z. Hong, Y. Yang, J. Kido, *Adv. Mater*, 2012, **24**, 2768.
14 G. Wei, S. Wang, K. Renshaw, M.E. Thompson, S.R. Forrest, *ACS Nano*., 2010, **4**, 1927.
15 G. Wei, S. Wang, K. Sun, M.E. Thompson, S.R. Forrest, *Adv. Energy Mater.,* 2011, **1**, 184.
16 D. Bagnis, L. Beverina, H. Huang, F. Silvestri, Y. Yao, H. Yan, G.A. Pagani, T.J. Marks, A. Facchetti, *J. Am. Chem. Soc*., 2010, **132** , 4074.
17 Z. He, C. Zhong, S. Su, M. Xu, H. Wu, Y. Cao, *Nature Photon*., 2012, **6**, 591.
18 R. Xia, D.-S. Leem, T. Kirchartz, S. Spencer, C. Murphy, Z. He, H. Wu, S. Su, Y. Cao, J.S. Kim, J.C. de Mello, D.D.C. Bradley, J. Nelson, Adv. Energy Mater., 2013, **3**, 718.
19 H.J. Snaith, *Nat Photon*, 2012, **6** , 337.
20 E. Zimmermann, P. Ehrenreich, T. Pfadler, J.A. Dorman, J. Weickert, L. Schmidt-Mende, *Nat Photon*, 2014, **8**, 669.
21 N. J. Turro, *Modern Molecular Photochemistry*, 1991
22 A. H. Abou El Ela, H. H. Afifi. *Phys. Chem. Solids*. 1979, **40**. 257.
23 B. Ebenhoch, S.A.J. Thomson, K. Genevicius, G. Juška, I. D.W. Samuel, *Org. Electron*. 2015, **22** , 62.
24 P. Cheng, Y. Li, X. Zhan, *Energy Environ. Sci*., 2014, **7**, 2005.
25 P. W. M. Blom, M. J. M. de Jong, J. J. M. Vleggaar, *Appl. Phys. Lett.* 1996, **68**, 3308
26 P Schilinsky, C. Waldauf, C.J. Brabec , *Appl. Phys. Lett*., 2002, **81** , 3885.
27 V. D. Mihailetchi, J. Wildeman, P. W. M. Blom, *Phys. Rev. Lett.*, 2005, 94, 126602.
28 J.C. Blakesley, D. Neher, *Phys. Rev. B*, 2011, **84** ,075210.
29 B.P. Rand, D.P. Burk, S.R. Forrest, *Phys. Rev. B*, 2007, **75**, 115327.
30 C-Y Nam, *J. Phys. Chem. C,* 2014, **118**, 27219.